Nuclear Engineering and Technology 53 (2021) 3966–3978

Contents lists available at ScienceDirect

Nuclear Engineering and Technology

journal homepage: www.elsevier.com/locate/net

Original Article

Validation of the correlation-based aerosol model in the ISFRA sodium-cooled fast reactor safety analysis code

Churl Yoon [a, *], Sung Il Kim [b], Sung Jin Lee [c], Seok Hun Kang [a], Chan Y. Paik [c]

[a] Versatile Reactor Technology Development Division, Korea Atomic Energy Research Institute, 111 Daedeok-daero 989 Beon-gil, Yuseong-gu, Daejeon, 34057, Republic of Korea
[b] Accident Mitigation Research Team, KAERI, Republic of Korea
[c] Fauske & Associates, LLC, 16W070 83rd, Street, Burr Ridge, IL, 60527, USA

ARTICLE INFO

Article history:
Received 22 September 2020
Received in revised form
20 June 2021
Accepted 22 June 2021
Available online 25 June 2021

Keywords:
Sodium-cooled fast reactor (SFR)
Severe accident
Fission product
Aerosols
Log-normal distribution

ABSTRACT

ISFRA (Integrated SFR Analysis Program for PSA) computer program has been developed for simulating the response of the PGSFR pool design with metal fuel during a severe accident. This paper describes validation of the ISFRA aerosol model against the Aerosol Behavior Code Validation and Evaluation (ABCOVE) experiments undertaken in 1980s for radionuclide transport within a SFR containment. ABCOVE AB5, AB6, and AB7 tests are simulated using the ISFRA aerosol model and the results are compared against the measured data as well as with the simulation results of the MELCOR severe accident code. It is revealed that the ISFRA prediction of single-component aerosols inside a vessel (AB5) is in good agreement with the experimental data as well as with the results of the aerosol model in MELCOR. Moreover, the ISFRA aerosol model can predict the "washout" phenomenon due to the interaction between two aerosol species (AB6) and two-component aerosols without strong mutual interference (AB7). Based on the theory review of the aerosol correlation technique, it is concluded that the ISFRA aerosol model can provide fast, stable calculations with reasonable accuracy for most of the cases unless the aerosol size distribution is strongly deformed from log-normal distribution.

1. Introduction

Since 1987 Korea Atomic Energy Research Institute (KAERI) has been developing a design and analysis technique for a pool-type sodium-cooled fast reactor called Prototype Gen-IV Sodium-cooled Fast Reactor (PGSFR). The PGSFR design focuses on the inherent safety characteristics of metal fuel and passive cooling using natural circulation and thermal expansion [1].

Despite the extremely low probability of a severe accident expected in the PGSFR due to the inherent safety characteristics and design features such as the passive shutdown system and passive decay heat removal system, the analytical capabilities and tools to predict release and transport of radioactive fission products (FPs) from the core to the containment and release to the environment under postulated nuclear power plant accidents are required for public acceptance and licensing. To this end, KAERI and Fauske & Associates, LLC (FAI), jointly developed the Integrated Sodium Fast Reactor Analysis (ISFRA) computer program to simulate the response of the PGSFR pool design with metal fuel during a severe accident. ISFRA was designed to be a fast-running simulation software used to predict the initial transient and the subsequent release and transport of FPs in a PGSFR [2].

The ISFRA computer program adopts the aerosol correlation technique of Epstein et al. [3–6] to predict behavior of non-volatile fission product (FP) aerosols inside a primary coolant system and containment under postulated severe accident conditions, tracking the suspended and deposited aerosol masses. As an integrated reactor analysis program developed specifically for PGSFR, the ISFRA code consists of thermal-hydraulics model, reactor kinetics model and various component models covering a core, a vessel, heat exchangers, containments et al.

Since the PGSFR uses liquid sodium as a coolant, in the event of coolant boiling and leakage into the containment, a sodium fire would occur and produce a large amount of sodium oxide aerosols,

* Corresponding author.
E-mail address: cyoon@kaeri.re.kr (C. Yoon).

https://doi.org/10.1016/j.net.2021.06.036

which will coagulate with FP aerosols that were leaked into the containment. Therefore, the behavior of FP aerosols inside the containment and release to the environment will be strongly affected by the presence of sodium oxide aerosols. In the ABCOVE experiments [7–9] sodium oxide aerosols were generated by a sodium spray/pool fire. Then, sodium iodide (NaI) aerosols were released in the presence of sodium combustion product aerosols. ABCOVE AB5, AB6, and AB7 tests are simulated using the ISFRA aerosol model and the results are compared against the measured data as well as with the simulation results of the MELCOR severe accident code.

The purpose of this study is to assess the capabilities and limitations of the aerosol model in the ISFRA code. In Section 2, the governing equations, assumptions, and derivation of the ISFRA aerosol model are reviewed. In the subsequent sections, the aerosol model is validated against the ABCOVE experiments to identify the capabilities and limitations of the ISFRA aerosol model.

2. ISFRA aerosol model

The theory behind the aerosol correlation technique of Epstein et al. [3–6] and the implementation of the technique in the ISFRA aerosol model is reviewed in this section. The advantages and limitations of the ISFRA aerosol model is discussed in Section 2.6.

2.1. Governing equation

The time rate of the suspended aerosol concentration in an arbitrary control volume can be derived by balancing the various mechanisms through which aerosols can be gained or lost from the volume. When $n(v, t)$ is the particle size distribution function, n (v, t)dv represents the number concentration of particles in the particle volume range v to $v + dv$ at time t. The equation governing $n(v, t)$ for an aerosol supplied with particles at the constant rate $\dot{n}_p(v)$ and losing mass by deposition on surrounding surfaces at a velocity $u(v)$ is as follows [3].

$$\frac{\partial n(v,t)}{\partial t} = \frac{1}{2}\int_0^v K(\bar{v}, v-\bar{v}) n(\bar{v},t) n(v-\bar{v},t) d\bar{v} - \int_0^\infty K(\bar{v}, v) n(\bar{v},t) n(v,t) d\bar{v} - \frac{n(v,t)u(v)}{h} + \dot{n}_p(v) \tag{1}$$

where $K(v, \bar{v})$ is the kernel representing the frequency of binary collisions between particles of volume v and $\bar{v}$, and h is the effective height for deposition of the aerosol (= cloud volume/surface area).

The functional form for the collision kernel $K(v, \bar{v})$ that appears in Eq. (1) depends on the coagulation mechanisms assumed to govern the behavior of the aerosol. Since the major mechanisms causing particle collisions in an enclosed compartment are Brownian motion of the particles and gravitational settling, the collision kernel can be expressed as follows:

$$K(v,\bar{v}) = K_B(v,\bar{v}) + K_g(v,\bar{v}) \tag{2}$$

where $K_B(v, \bar{v})$ and $K_g(v, \bar{v})$ represent the collision kernels for the Brownian and gravitational coagulation mechanisms, respectively.

For particles larger than the gas mean free path, the collision kernels for the Brownian and gravitational coagulation mechanisms, written in terms of particle volume, are

$$K_B(v,\bar{v}) = \frac{\gamma K_0}{2\chi}\left(v^{1/3} + \bar{v}^{1/3}\right)\left(v^{-1/3} + \bar{v}^{-1/3}\right) \tag{3}$$

$$K_g(v,\bar{v}) = \frac{2\pi g \rho \gamma^2}{9\mu\alpha^{1/3}\chi}\varepsilon(v,\bar{v})\left(\frac{3}{4\pi}\right)^{4/3}\left(v^{1/3} + \bar{v}^{1/3}\right)^3\left|\bar{v}^{1/3} - v^{1/3}\right| \tag{4}$$

where ρ is the density of the aerosol material, μ is the viscosity of the gas in which the particles are suspended, and K_0 (= $4kT/(3\mu)$) is the normalized Brownian collision coefficient. Here, α is the density correction factor, γ is the collision shape factor, and χ is the particle settling shape factor. $\varepsilon(v, \bar{v})$ is the capture coefficient, which is in the following functional form [10].

$$\varepsilon(v,\bar{v}) = \frac{3}{2}\left(\frac{v^{1/3}}{v^{1/3} + \bar{v}^{1/3}}\right)^2 \tag{5}$$

Taking the first moment of Eq. (1) to temporarily avoid the many complications, Eq. (1) becomes the ordinary differential equation for the density of the suspended mass, m

$$\frac{dm(t)}{dt} = -\lambda(t) m(t) + \dot{m}_p \tag{6}$$

Here, m is the total mass concentration expressed as

$$m(t) = \rho\int_0^\infty v n(v,t) dv \tag{7}$$

The constant mass rate of production of aerosol particles per unit volume, $\dot{m}_p$, is

$$\dot{m}_p(t) = \rho\int_0^\infty v \dot{n}_p(v,t) dv \tag{8}$$

And, λ is the aerosol removal rate constant defined as

$$\lambda(t) = \frac{\int_0^\infty v n(v,t) u(v) dv}{h\int_0^\infty v n(v,t) dv} \tag{9}$$

2.2. Aerosol similitude and similarity analysis

In the consequence analyses of postulated nuclear power plant accidents, we have to track the total suspended mass and the particle size distribution of aerosols undergoing Brownian coagulation and gravitational settling. Previous work with Eq. (1) has shown that as time progresses, the particle size distribution becomes independent of the initial distribution. It has been also shown theoretically that particle size spectra of aerosols coagulating by Brownian motion reach a constant “self-preserving form” (with respect to particle size) independent of the initial distribution after a sufficiently long time [3,4]. The tendency for aerosols to approach a certain size distribution is called “aerosol similitude.” The aerosol similitude can be achieved by selecting suitable scale factors for the particle number density, particle volume, and time.

2.2.1. For aging aerosols

To avoid the complexity of the above governing equations, Epstein et al. [3] transformed the aerosol equations to

dimensionless forms that readily reveal the nature of the similarities that exist among seemingly different aerosols. "Similarity" means that as time increases the particle size distribution becomes independent of the initial particle size distribution. For aging aerosols, $\dot{n}_p(v) = 0$, and the governing equations are reduced to a set of universal forms by introducing the dimensionless particle volume v, dimensionless time τ, and dimensionless particle distribution function $N(v, \tau)$ as following:

$$n(v,t) = c_1 N(v,\tau),\ v = c_2 v,\ \text{and}\ t = c_3 \tau, \tag{10}$$

By solving the governing equations for c_1, c_2, and c_3, the quantities of $m(t)$, $\lambda(t)$, and $\dot{m}_p$ can be transformed into the dimensionless total density of the suspended aerosol $M(\tau)$, dimensionless removal constant $\Lambda(\tau)$, and the dimensionless particle source strength $\dot{M}_p$.

Finally, the settling velocity for the small particles of interest in aerosol transport is accurately represented by Stokes' law. Stokes' law written in terms of particle volume and corrected for non-spherical or porous particles is [3].

$$u(v) = \frac{2}{9}\left(\frac{3}{4\pi}\right)^{2/3} \cdot \frac{\alpha^{1/3} g \rho v^{2/3}}{\chi \mu} \tag{11}$$

Substituting Eqs. (2)–(4) and (10) and (11) into Eq. (1), one can obtain the unknowns c_1, c_2, and c_3 through dimensional analysis [3,11]:

$$\begin{aligned} c_1 &= \left(\frac{\alpha g^5 \rho^5}{\gamma^3 K_0{}^5 \mu^5 h^4}\right)^{1/4}; \\ c_2 &= \left(\frac{\alpha^{1/3} \mu K_0}{\gamma g \rho}\right)^{3/4}; \\ c_3 &= \left(\frac{\chi^2 \gamma \mu h^2}{\alpha g \rho K_0}\right)^{1/2}. \end{aligned} \tag{12}$$

On the other hand, the dimensionless total suspended aerosol mass M is transformed from $m(t)$:

$$\begin{aligned} M(\tau) &= \int_0^\infty v N(v,\tau) dv = \frac{1}{c_1 c_2^2} \int_0^\infty v n(v,t) dv \\ &= \left(\frac{\gamma^9 g h^4}{\alpha^3 K_0 \mu \rho^3}\right)^{1/4} \cdot m(t) \end{aligned} \tag{13}$$

The dimensionless decay constant is defined and expressed as

$$\Lambda(\tau) = \frac{\int_0^\infty v^{(1+2/3)} N(v,\tau) dv}{\int_0^\infty v N(v,\tau) dv} = \left(\frac{\gamma \chi^2 \mu h^2}{\alpha K_0 g \rho}\right) \cdot \lambda \tag{14}$$

2.2.2. For steady-state aerosols

The particle size distribution of an aerosol continually reinforced by the introduction of particles at a steady rate and losing particles by sedimentation will ultimately achieve an equilibrium condition in which $\partial n(v,t)/\partial t = 0$. Here, time does not enter into the coagulation equation, but of course the source term $\dot{n}_p(v)$ must be retained. It can readily be shown by the method in the preceding section that the scaling factors for the quantities n, v, and m of an aerosol in steady-state are given by Eqs. (10), (12) and (13). Similar transformations can be derived by introducing the dimensionless parameters v, τ, $N(v, \tau)$, and an additional dimensionless particle source rate $\dot{N}_p(v)$:

$$\begin{aligned} n(v,t) &= d_1 N(v,\tau), \\ v &= d_2 v, \\ t &= d_3 \tau, \ \text{and} \\ \dot{n}_p(v) &= d_4 \dot{N}_p(v) \end{aligned}$$

Substituting these equations into Eq. (1) with $\partial n(v,t)/\partial t = 0$, dimensional analysis gives algebraic compatibility equations for the coefficients d_1, d_2, d_3, and d_4 similar to the aging aerosol case. Solving these algebraic equations, we obtain the transformations as follows.

$$d_1 = c_1,\ d_2 = c_2,\ d_3 = c_3$$

From the dimensional analysis of the source term in RHS of the governing equation

$$\begin{aligned} d_4 = \frac{d_1}{d_3} &= \left(\frac{\alpha g^5 \rho^5}{\gamma^3 K_0{}^5 \mu^5 h^4}\right)^{1/4} \left(\frac{\alpha^2 g^2 \rho^2 K_0{}^2}{\chi^4 \gamma^2 \mu^2 h^4}\right)^{1/4} \\ &= \left(\frac{\alpha^3 g^7 \rho^7}{\gamma^5 \chi^4 K_0{}^3 \mu^7 h^8}\right)^{1/4} \end{aligned}$$

Therefore, the dimensionless particle production rate is

$$\dot{N}_p(v) = \left(\frac{\gamma^5 \chi^4 K_0{}^3 \mu^7 h^8}{\alpha^3 g^7 \rho^7}\right)^{1/4} \cdot \dot{n}_p(v) \tag{15}$$

A physically more significant parameter is the dimensionless total mass introduction rate of particles $\dot{M}_p$, which can be related directly to $\dot{N}_p(v)$ by Eq. (8)

$$\dot{M}_p = \left(\frac{\gamma^{11} \chi^4 \mu h^8}{\alpha^5 g K_0^3 \rho^5}\right)^{1/4} \dot{m}_p = \int_0^\infty v \dot{N}_p(v) dv \tag{16}$$

The non-dimensional form of major variables so far derived for aging (decaying) and steady-state aerosols undergoing Brownian and gravitational coagulation and settling are summarized in Table 1. It should be noted that the scaling factors in the table do not include any of the properties of the initial distribution.

The results of numerical calculations for the evolution of the sectionalized particle mass distributions at dimensionless aging times $\tau = 0.2$, 1.0, and 2.0 for two different aerosols losing mass by sedimentation are shown in Fig. 1. The MAEROS numerical technique [12,13] was used for the calculations, which is based on dividing the particle size domain into sections and dealing with one integral quantity in each section. Thus, MAEROS calculations give information of the transient aerosol size distribution and composition as outputs. The MAEROS code used for the calculation was provided from the OECD/NEA data bank system [14]. The initial

Table 1
Non-dimensional form of major variables for aerosols undergoing Brownian. and gravitational coagulation and settling.

Time, τ	Particle volume, υ	Particle number density, N
$\left(\frac{\alpha g \rho K_0}{\chi^2 \gamma \mu h^2}\right)^{1/2} \cdot t$	$\left(\frac{\gamma g \rho}{\alpha^{1/3} \mu K_0}\right)^{\frac{3}{4}} \cdot v$	$\left(\frac{\gamma^3 K_0{}^5 \mu^5 h^4}{\alpha g^5 \rho^5}\right)^{1/4} \cdot n$
Mass density, M	**Decay constant, Λ**	**Particle production rate, $\dot{N}_p$**
$\left(\frac{\gamma^9 g h^4}{\alpha^3 K_0 \mu \rho^3}\right)^{\frac{1}{4}} \cdot m$	$\left(\frac{\gamma \chi^2 \mu h^2}{\alpha K_0 g \rho}\right)^{1/2} \cdot \lambda$	$\left(\frac{\gamma^5 \chi^4 K_0{}^3 \mu^7 h^8}{\alpha^3 g^7 \rho^7}\right)^{\frac{1}{4}} \cdot \dot{n}_p$

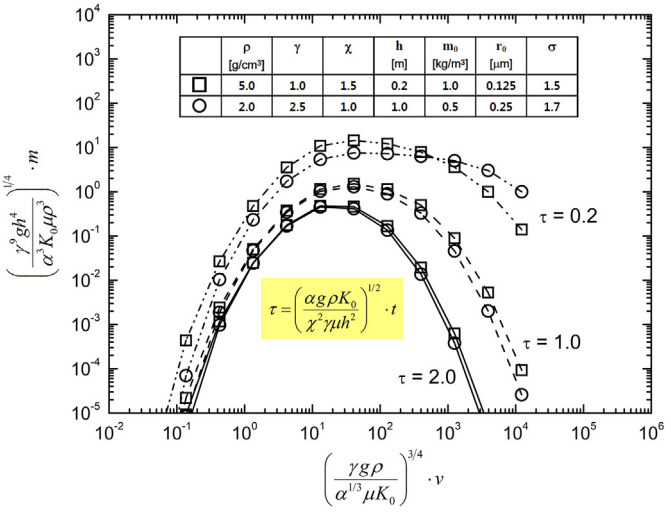

Fig. 1. Particle mass distribution at dimensionless aging times τ = 1.0 and 2.0 of two different aerosols losing mass by sedimentation and undergoing Brownian and gravitational coagulation (Reproduction of Fig. 1 in Ref. [4]).

particle size spectra were taken to be of the log-normal form. In Fig. 1, the aerosols with different initial size distributions and properties have a more similar dimensionless particle size spectrum at the larger dimensionless time. Therefore, it is clearly shown in Fig. 1 that the similarity principle is approached after sufficient time has passed so that the individual peculiarities related to the initial distribution of a particular aerosol are forgotten.

2.3. Correlations for aerosol sedimentation

To determine the functional relationships $\Lambda(M)$, FAI obtained empirical fitting equations based on many numerical solutions and experimental data [2,15]. Numerical solutions are obtained again by running a sectional analysis tool, the MAEROS code, which was developed by Gelbard et al. [12,13]. Fig. 2 shows the dimensionless removal rate constant as a function of dimensionless suspended aerosol mass concentration, from the measured aerosol mass concentrations of the ABCOVE experiments and several numerical experiments using the MAEROS code. This figure is a reproduction of the similar concept of Fig. 1 in Epstein et al. [5].

From the calculated and measured data in Fig. 2, two fitting curves are obtained by FAI. The lower dashed curve corresponds to aerosols continually supplied with particles, under steady-state conditions, in which the loss of particle mass by gravitational sedimentation is balanced by the constant rate of input of particle mass. The upper solid curve is the dimensionless removal rate versus dimensionless mass concentration relation for decaying aerosols in the absence of a source. The obtained algebraic fit equations for the curves are

$$\Lambda_{SED}^{SS} = 0.266 M^{0.282}\left(1 + 0.189 M^{0.8}\right)^{0.695} \tag{17}$$

$$\Lambda_{SED}^{D} = 0.528 M^{0.235}\left(1 + 0.473 M^{0.754}\right)^{0.786} \tag{18}$$

Here, superscript *SS* indicates when the removal rate constant refers to steady-state conditions, superscript *D* denotes Λ for a decaying aerosol, and subscript *SED* denotes particle removal by sedimentation.

For the MAEROS numerical experiments, the aerosol size distribution is divided into 30 sectional bins of the particle diameter

SYMBOL	h [m]	$\dot{m}_p$ [kg/m³/s]	ρ [kg/m³]	γ	χ	σ	r₀ [μm]
□	3.1017	9.1549E-7	2450	2.25	1.5	2.0	0.125
△	10.0	8.2160E-6	4000	2.5	1.0	1.55	0.136
○	3.1017	5.9038E-6	2130	2.25	1.5	2.0	0.25
◇	5.0	2.3122E-4	5000	1.0	1.0	1.55	0.27
▽	3.1017	1.1737E-4	3670	2.25	1.5	2.0	0.5
X	2.0	2.9343E-5	2000	1.0	1.0	2.5	1.0
⬡	1.0	1.1737E-4	1000	1.0	1.0	1.5	0.5

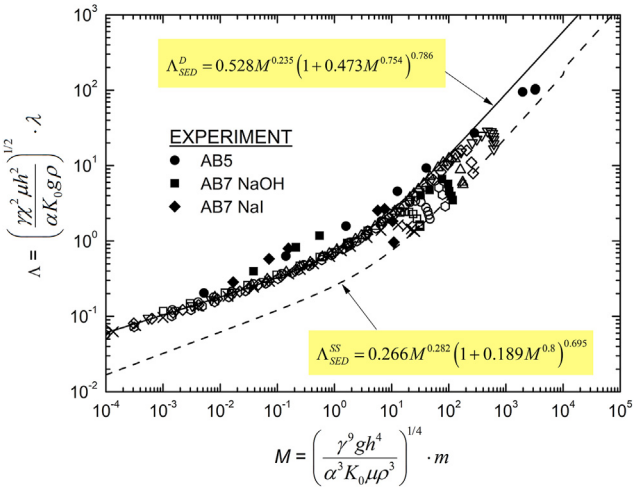

Fig. 2. Dimensionless aerosol removal rate constant for sedimentation as a function of dimensionless suspended mass concentration; steady-state and aging aerosol curves and experimental data (Reproduction of Fig. 1 in Ref. [5]).

ranging from 0.01 μm to 250 μm. Aerosol particle source rates with log-normal source distributions having standard deviations σ and initial geometric mean particle diameters d_0 are applied for a certain period of time and then turned off ($\dot{m}_p = 0$). In the MAEROS code, the gravitational settling velocity is expressed as

$$u(d_p) = \frac{d_p^2 g \rho C_m}{18 \chi \mu} \tag{19}$$

The gravitational settling velocity in Eq. (19) is expressed by the aerosol particle diameter d_p, while that of Eq. (11) is expressed by the aerosol volume *v*. Since both the Cunningham slip correction factor C_m in Eq. (19) and the density correction factor α in Eq. (11) are estimated to be around 1, Eqs. (11) and (19) are essentially the same [16]. In numerical experiments, the particle deposition onto walls by thermophoresis and diffusion mechanisms are removed by giving zero air-to-wall temperature gradients and very large diffusion boundary layer thicknesses as input parameters. The resultant values of volumetric suspended aerosol mass and particle number in each size sections, from the MAEROS simulations, are manipulated to generate dimensionless decay constants as a function of dimensionless suspended aerosol mass concentrations. In estimating the dimensionless decay constant Λ by Eq. (14), the decay constants λ are obtained from the MAEROS numerical solutions through Eq. (9).

For the ABCOVE measured data, the suspended NaO_x aerosol mass concentrations of the ABCOVE AB5 test and the suspended NaI and NaOH aerosol mass concentrations of the ABCOVE AB7 test are converted to dimensionless suspended aerosol mass concentration M and the corresponding dimensionless removal constant Λ by Eqs. (13) and (14). The ABCOVE AB6 data are not used because these data have a strong interaction between the NaI and NaO_x aerosols,

which will be discussed in Section 4.2. For these experimental data, since the airborne aerosol removal is caused by the turbulent deposition due to natural convection inside the vessel and the thermophoretic deposition due to air-to-wall temperature differences as well as gravitational sedimentation, the values of dimensionless aerosol removal rate constant Λ are higher than those of numerical experiments. Thus, the algebraic fitting equations of Eqs. (17) and (18) are obtained based on the numerical solutions only, because the aerosol deposition owing to gravitational settling without any other deposition mechanisms is considered here.

After the dimensionless decay constant Λ is calculated from the dimensionless suspended aerosol mass concentration M by using Eq. (17) or (18) for steady-state or decaying aerosols, the dimensionless decay constant Λ is transformed into an aerosol removal rate constant λ by utilizing Eq. (14). Steady-state and decaying conditions are expressed as

$$\frac{dm(t)}{dt} = -\lambda_{SED}^{SS} m(t) + \dot{m}_p \tag{20}$$

$$\frac{dm(t)}{dt} = -\lambda_{SED}^{D} m(t) \tag{21}$$

Here again, superscript *SS* indicates when the removal rate constant refers to steady-state conditions, superscript *D* denotes Λ for a decaying aerosol, and subscript *SED* denotes particle removal by sedimentation.

To switch from one of the decaying or the steady-state correlation to another, the FAI correlation-based aerosol model uses an interpolation factor (*FSEDDK*) between decaying and steady-state correlations. One can get the expected steady-state airborne aerosol mass m^{ss} from Eq. (6), assuming the time derivative term is eliminated.

$$m^{ss} = \frac{\dot{m}_p}{\lambda_{SED}}$$

When there is no aerosol source, $\lambda_{SED} = \lambda_{SED}^{D}$ and the airborne aerosol mass concentration is calculated from Eq. (21). For the cases that there are aerosol sources, two conditions exist depending on whether the current suspended aerosol mass m(t) is larger than the steady-state airborne aerosol mass m^{ss} or not. When (m(t)/m^{ss}) is smaller than 1.0 with aerosol sources, $\lambda_{SED} = \lambda_{SED}^{SS}$ and the airborne aerosol mass concentration is calculated from Eq. (20). When (m(t)/m^{ss}) is larger than 1.0 with aerosol sources, the interpolation factor (*FSEDDK*) is estimated from 0 to 1.0 for the varying (m(t)/m^{ss}) value from 1.0 to 8.0. Then, the airborne aerosol mass concentration is obtained by using Eq. (20) with the following removal rate constant.

$$\lambda_{SED} = FSEDDK * \lambda_{SED}^{D} + (1 - FSEDDK) * \lambda_{SED}^{SS}$$

2.4. Correlations for other deposition mechanisms

In addition to the gravitational settling, other deposition mechanisms of airborne aerosols in a confined compartment are turbulent deposition and inertial impaction, when there is no other force on particles such as electrostatic forces.

For the case of aerosol particles in high-velocity forced flow, the rate of turbulent deposition onto walls can be comparable to the deposition by sedimentation. The turbulence aerosol deposition velocity in a pipe flow is given by

$$u(\nu) = 4.21 \times 10^{-7} f^{1/2} u_g \left(\frac{f u_g^2 \rho_g \alpha^{1/3} \rho \nu^{2/3}}{\chi \mu^2} \right)^2 \tag{22}$$

where u_g and ρ_g are the gas velocity and density, respectively, and f is the friction factor for turbulent flow. The shape factors χ and α correct the Stokesian resistance for the penetration of porous or non-spherical particles, respectively. By replacing Eq. (11) with Eq. (22) in the derivation in Section 2.2, the analogous expression for aerosol decay by turbulent deposition was obtained. By running the sectional aerosol code MAEROS with the deposition velocity given by Eq. (22), the correlations of the dimensionless suspended aerosol mass and removal rate constant are obtained as shown in Table 2.

Flow obstructions such as pipe bends, a sudden contraction, steam separators, or steam dryers can lead to aerosol impaction on surfaces. The inertial impaction deposition velocity on a body of diameter D is given by

$$u(\nu) = E \cdot u_g = 0.068 \left(\frac{\rho \alpha^{1/3}}{\chi \mu D} \right)^{2/3} u_g^{5/3} \nu^{4/9} \tag{23}$$

where E is the efficiency of inertial impaction deposition defined as the ratio of the number of particles that actually reach the body to the number of particles that would have reached it had they

Table 2
Correlations for aerosol deposition mechanisms.

Deposition Process	Aerosol Mass Density, M	Removal Rate Constant, Λ	Correlations
Sedimen-tation	$\left(\frac{\gamma^9 g h^4}{\alpha^3 K_0 \mu \rho^3}\right)^{\frac{1}{4}} \cdot m$	$\left(\frac{\gamma \chi^2 \mu h^2}{\alpha K_0 g \rho}\right)^{1/2} \cdot \lambda$	Steady-State: $\Lambda = 0.266 M^{0.282}(1 + 0.189 M^{0.8})^{0.695}$ Decay: $\Lambda = 0.528 M^{0.235}(1 + 0.473 M^{0.754})^{0.786}$
Turbulent Flow	$\left(\frac{\gamma K_0 h \mu^4}{\chi f^{5/2} \rho^3 \rho_g^2 u_g^5}\right) \cdot \left(\frac{\gamma g \rho}{\alpha^{1/3} \mu K_0}\right)^{7/4} \cdot m$	$\left(\frac{\gamma g h}{\alpha^{1/3} f^{5/2} K_0}\right) \cdot \left(\frac{\mu^3}{u_g^5 \rho_g^2 \rho}\right) \cdot \lambda$	Steady-State: $\Lambda = 3.04 \times 10^{-3} M^{0.606}(1 + 4.16 \times 10^3 M^{1.36})^{0.25}$ Decay: $\Lambda = 4.06 \times 10^{-3} M^{0.512}(1 + 3.07 \times 10^3 M^{1.106})^{0.397}$
Inertial Impaction	$\left(\frac{\gamma K_0 h}{\chi \rho u_g}\right)\left(\frac{\mu D}{\rho u_g}\right)^{2/3} \cdot \left(\frac{\gamma g \rho}{\alpha^{1/3} \mu K_0}\right)^{13/12} \cdot m$	$\left(\frac{h}{u_g}\right)\left(\frac{\mu D}{\rho u_g}\right)^{2/3} \cdot \left(\frac{\gamma g \rho}{\alpha^{1/3} K_0 \mu}\right)^{1/3} \cdot \lambda$	Steady-State: $\Lambda = 0.126\, M^{0.26}(1 + 2.92\, M^{1.28})^{0.137}$ Decay: $\Lambda = 0.337\, M^{0.21}(1 + 1.74\, M^{1.9})^{0.14}$
Leakage	–	$\frac{h_L \lambda_L}{u_L}$	Steady-State or Decay:. $\Lambda = 1$

continued in a straight line rather than follow the streamlines. By replacing Eq. (11) with Eq. (23) in Section 2.2, the treatment used for aerosol sedimentation can be repeated for the inertial deposition.

So far in this study, aerosol particle coagulation and deposition in a confined compartment has been considered. In practice, there could be transportation of aerosols and carrier gases between compartments (i.e., control volumes), which finally lead to leakage to the environment. Thus, we next consider the additional complication of aerosol leakage as a result of bulk flow of gas from the volume. Assuming all particles flow from the volume with the carrier gas velocity through the leak, the leakage mass flux of particulate can then be calculated from the mass continuity expression

$$\left.\frac{dm}{dt}\right|_{leak} = -\frac{u_L m}{h_L} \tag{24}$$

where the quantity h_L is the effective height of the particle cloud relevant to leakage, which equals the leak flow area divided by the volume of the compartment. When we consider particle leakage as simply another deposition mechanism that acts in isolation, the removal rate constant for particle leakage becomes

$$\lambda_L = -\frac{u_L}{h_L} \tag{25}$$

Since λ_L is independent of the shape of the particle size distribution, Eq. (25) is valid for all regimes of aerosol behavior, including steady-state and pure decay.

Table 2 summarizes expressions for the dimensionless parameters and correlations between them for the cases of sedimentation deposition, turbulent deposition, inertial deposition, and leakage.

2.5. Correlations for simultaneous multiple deposition mechanisms

For aerosols with multiple deposition mechanisms, the mass balance equation of Eq. (6) can be generalized as

$$\frac{dm}{dt} = -\lambda_{TOT} m + \dot{m}_p \tag{26}$$

Here, λ_{TOT} is the total removal rate constant for combined aerosol removal mechanisms:

$$\lambda_{TOT} = \lambda^{\bullet}_{SED} + \lambda^{\bullet}_{\lambda_{IMP}} + \lambda^{\bullet}_{\lambda_{DIF}} + \lambda^{\bullet}_{\lambda_{TH}} \tag{27}$$

where the superscript black dot (•) indicates that the removal rate constant depends on other accompanying deposition processes. And, $\lambda^{\bullet}_{DIF}$ and $\lambda^{\bullet}_{TH}$ are removal rate constants due to diffusiophoresis and thermophoresis, respectively, in the presence of sedimentation. The removal rate constant for particle leakage λ_L does not appear in Eq. (27) since aerosol leakages are calculated with the implicit flow solver between nodes by the fractional-step method [17]. When simultaneous multiple deposition mechanisms occur the individual removal rate constants are corrected to consider presence of other removal mechanisms.

In the aerosol correlation technique, approximate combination laws permit prediction of aerosol removal rates when two removal mechanisms are operating simultaneously. In the ISFRA code, three cases of simultaneous multiple mechanisms are considered: sedimentation and leakage, inertial impaction and leakage, and sedimentation and inertial impaction. For each case, the correction correlations for $\lambda^{\bullet}_{SED}$ and $\lambda^{\bullet}_{I}$ were obtained from the given λ_{SED}, λ_I, and λ_L based on the numerical results of the sectional method.

While sedimentation and inertial impaction removal rates are particle size-dependent, steam condensation, thermophoresis, and diffusiophoresis deposition rates on structure surfaces are independent of particle size, like aerosol removal by leakage. Epstein et al. [6] developed the dimensionless form of the local thermophoretic particle flux and the deposition velocity (u_{TH}) as

$$Sh_x = \frac{(-j)x\rho_g}{\mu_g \beta N_\infty} = \frac{1-(\beta \mathrm{Pr})^{1.25T_w/T_\infty}}{1-(\beta \mathrm{Pr})^{1.25}} \cdot \left(\frac{T_\infty}{T_w} - 1\right) \cdot Nu_x \tag{28}$$

and

$$u_{TH} = Sh_x \cdot \frac{\mu_g}{\rho_g} \cdot \frac{\beta}{x} \tag{29}$$

Here, j is the particle deposition flux in numbers per unit area per second, and β is the dimensionless thermophoretic velocity coefficient. The removal rate by thermophoretic deposition is given by

$$\lambda_{TH} = u_{TH}/h \tag{30}$$

where h is effective height (= volume/area), similarly as other removal mechanisms. The deposition velocity due to thermophoresis can be treated as a leakage term in the presence of sedimentation with β equal to 0.40 [15].

2.6. Advantages and limitations of aerosol correlation technique

The ISFRA aerosol model, which is based on the aerosol correlation technique, provides fast and stable calculations and is based on rigorous analysis. The governing equations for simultaneously coagulating and settling (by gravity) aerosols are transformed into non-dimensional equations based on aerosol similitude, where the particle size distribution reaches a log-normal distribution independent of the initial size distribution after a sufficiently long time. Using the numerical results of the sectional method, two non-dimensional fits are obtained for the aerosol behavior, one for steady-state and another for decaying aerosols. Using these fits, correlations for multiple simultaneous deposition rates are derived. Approximate combination laws permit prediction of aerosol removal rates when two deposition mechanisms are operating simultaneously. Hence, it is necessary to numerically integrate a single ordinary differential equation to obtain the suspended aerosol mass concentration. On the other hand, the sectional method is computationally expensive and often unstable due to numerical stiffness. It involves solving $M \times S$ ordinary differential equations, where M is number of sections and S is number of species.

The aerosol correlation technique is restricted to single-component aerosols. It is used, however, for calculating the behavior of multicomponent aerosols by invoking the assumption of uniform coagglomeration in which particles of all sizes are assigned the instantaneous average composition of the aerosols.

Aerosol coagulation and deposition depend on particle sizes. Therefore, if there is strong source or sink of specific aerosol size, the aerosol similitude would not be maintained, and the aerosol correlation technique may not work well. For example, aerosols emerging from a suppression pool will assume different size distribution.

The aerosol correlation technique breaks down when aerosols grow or shrink by condensation or evaporation. Hygroscopic aerosols have a large affinity for water and grows in humid environment. Aerosol droplets produced into a dry atmosphere undergo rapid evaporation. In both cases the aerosol size is affected by processes other than coagulation.

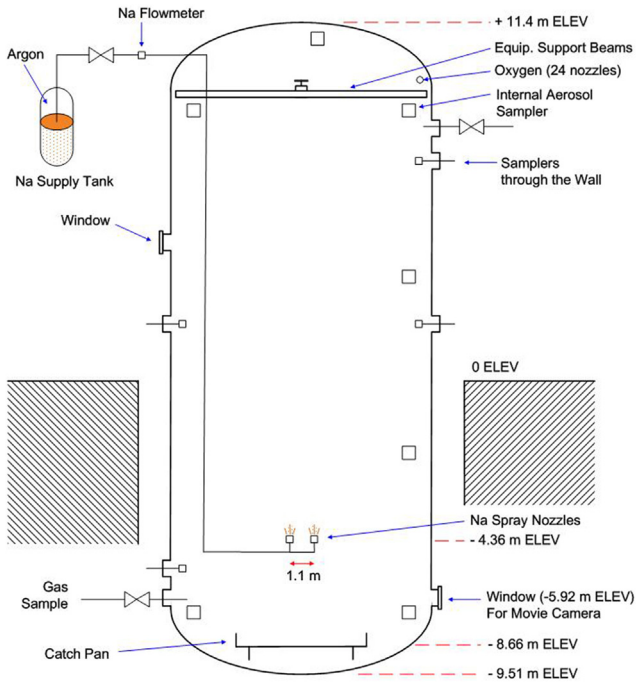

Fig. 3. CSTF vessel arrangement for test AB5.

3. ABCOVE experiments

The Aerosol Behavior Code Validation and Evaluation (ABCOVE) experiments were conducted under the LMFBR (Liquid-Metal Fast Breeder Reactor) Safety Program Plan [15], which was a cooperative effort between the U.S. Department of Energy, the U.S. Nuclear Regulatory Commission, and their contractors. A series of large-scale confirmatory tests were performed in the Containment Systems Test Facility (CSTF) vessel in the Hanford Engineering Development Laboratory (HEDL), covering a range of aerosol source release rates, source duration times, and complexity of aerosol composition. The CSTF vessel is a cylindrical steel tank (7.6 m diameter, 20.3 m high) of about 852 m^3 (Fig. 3). The vessel is furnished with instrumentation to monitor both thermal-hydraulics and aerosol behavior. Three experiments, AB5, AB6 and AB7, were used to validate the ISFRA aerosol model in this paper. The test conditions are summarized in Table 3.

Fig. 3 shows the CSTF vessel arrangement for the AB5 test. Test AB5 is a single-species aerosol test that involves spraying sodium at a high rate into an air atmosphere [15]. Aerosols were generated by a sodium spray fire. An amount of 223 kg of sodium was sprayed through two upward-facing nozzles located at −4.36 m from ground zero over a period of 872 s (from 13 to 885 s), with all the sodium converted to 60% Na_2O_2 and 40% NaOH aerosols. Oxygen was also injected so that the oxygen concentration remained relatively constant during this series of tests.

Test AB6 is an experiment for the case of a two-component aerosol simulating the release of a fission product (FP) in the presence of a sodium spray fire [8,18]. This experiment simulated an accident in which sodium iodide (NaI) aerosols were released in the presence of sodium combustion product aerosols. The main difference in test AB6 was a sodium iodide aerosol generator installed in a through-the-wall station at an elevation of −1.9 m. The NaI aerosols were injected into the containment vessel atmosphere at the rate of 0.14 g/s from 0 to 3000 s. Simultaneously, the sodium spray fire was produced by injecting commercial-grade sodium through a single spray nozzle located at an elevation of −4.36 m. The release rate of aerosols from the spray fire was approximately 500 times that of the NaI, and its source was continued well past the NaI source cutoff to demonstrate the "washout" of the NaI by the continuing sodium spray aerosols. A total amount of 204.7 kg of sodium was sprayed into the CSTF over a period of 4780 s (620~5400 s). All sodium was converted to NaOx aerosols consisting primarily of a mixture of sodium peroxide (Na_2O_2) and sodium hydroxide (NaOH).

Test AB7 is a NaI aerosol release test after the end of a small sodium pool fire [18]. The test involves release of the simulated FP, NaI, into the containment vessel atmosphere after the end of a small sodium pool fire. The primary purpose of test AB7 is to demonstrate the co-agglomeration behavior of two aerosol species under mild thermal conditions that minimize re-suspension and decomposition processes. Test AB7 was also performed in the CSTF vessel. Test AB7 began with the injection of sodium into the containment vessel. The sodium spraying line failed immediately after the initiation of the sodium flow. The failure was such that sodium leaked from the line and fell to the personnel deck at an elevation of −1.68 m, where it formed a pool and burned as a pool fire. The flow of sodium was stopped after 20 s. The duration of the pool fire is believed to be approximately 10 min (0~600 s). The sodium oxide aerosols that were released from the burning sodium were quickly converted to NaOH aerosols by reacting with moisture in the containment atmosphere. The NaI aerosols were released at 600 s with a constant rate of 0.197 g/s until 2400 s [19].

Table 3
Summary of ABCOVE test conditions.

Description	AB5	AB6	AB7
Initial CSTF Atmosphere Conditions			
Initial Atm. Temperature [K]	302.25	304.15	297.05
Initial Atm. Pressure [MPa]	0.122	0.114	0.118
Initial O_2 Concentration [vol%]	23.3 ± 0.2	23.9 ± 0.2	20.95
Initial Dew Point [K]	289.15 ± 2	285.35	274.65
Containment Condition During Test			
Maximum Avg. Atm. Temp. [K]	552.15	432.75	306.85
Maximum Avg. Steel Temp. [K]	366.65	352.05	298.35
Maximum Pressure [MPa]	0.214	0.170	0.123
Final O_2 Concentration [vol%]	19.4 ± 0.2	21.9 ± 0.2	20.25
Final Dew Point [K]	271.65	268.95	274.45
Na Spray/Spill (AB7) Conditions			
Na Spray/Spill Rate [g/s]	256 ± 15	42.8 ± 2.1	322
Na Spray/Spill Period [s]	13~885	620~5400	20~600
Na Sprayed/Delivered Mass [kg]	223 ± 11	204.7 ± 4.1	6.434
Na Initial Temperature [K]	836.15	833.15	863.15
NaI Aerosol Release Conditions			
NaI Release Rate [g/s]	_	0.14 ± 0.028	0.197
NaI Spray Period [s]	_	0~3000	600~2400
NaI Released Mass [g]	_	416	354.6
Source 50% diameter [μm]	_	0.543	0.54
Source GSD[a]	_	1.55	1.55

[a] GSD = Geometric Standard Deviation.

4. Simulation results and discussions

4.1. ABCOVE AB5 test

4.1.1. Simulation models

Since the ISFRA computer program was developed for PGSFR accident analysis, in order to treat the ABCOVE test section (CSTF vessel) and test conditions the subroutines comprising the aerosol model were extracted from the ISFRA program and a driver was created to handle inputs containing arbitrary geometries and boundary conditions. The stand-alone computer program comprised of ISFRA aerosol routines and the driver was used for the entire validation processes.

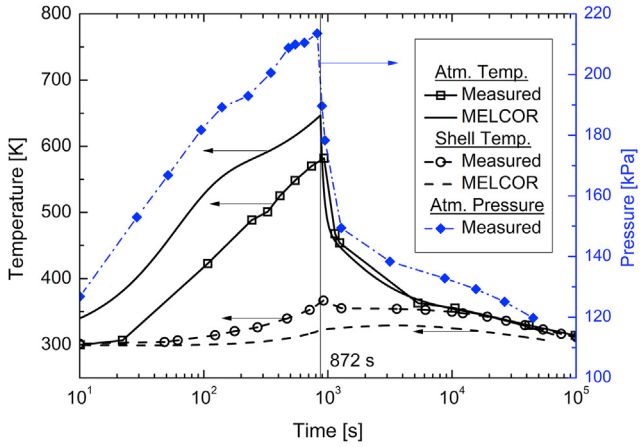

(a) CSTF atmosphere temperature, pressure, and shell temperature

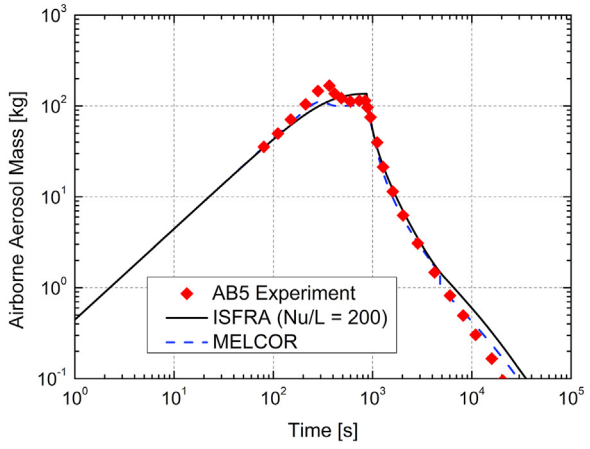

(b) Suspended aerosol mass inside the CSTF

Fig. 4. Validation condition and results for the AB5 test.

For the aerosol analyses of the AB5 test using ISFRA, the CSTF vessel was modeled as a single control volume containing atmospheric air and aerosols. During a sodium spray fire, the measured gas temperature increased and reached the maximum temperature of 533 K at the end of the sodium spray (885 s). After that, the gas temperature decreased without any sodium fire. The measured CSTF shell and atmosphere temperatures (Fig. 4(a)) were provided as input to ISFRA as functions of time. Fig. 4(a) also shows the CSTF shell and atmosphere temperatures calculated by the MELCOR runs made by one of the authors [20]. These presented shell temperatures calculated by MELCOR are the average values of inner and outer surface temperatures. The addition of aerosol mass induced by the sodium spray fire for 872 s (from 13 to 885 s) was modeled as a constant aerosol mass source rate of 0.445 kg/s into the 852.0 m^3 control volume. The time-step sizes for the ISFRA runs were directly controlled by user input, starting with a small time-step and increasing with time.

For aerosol analysis using the sectional method (MELCOR), the containment thermal-fluidic subroutines were included. However, some thermal-hydraulic conditions were controlled by the tabular function in MELCOR, such as enthalpy addition in the vessel and heat structure outer wall temperatures. Since the thermal-hydraulics calculation could not reproduce the measured CSTF temperature and pressure, probably due to heat losses to the outer wall, presence of aerosols, and incorrect chemical reaction model for the sodium spray fire, imposing some thermal-hydraulic conditions would be helpful to validate the aerosol portion of the model against experiments. The measured CSTF shell and atmosphere temperatures were provided as input to the MELCOR calculation, similar to the ISFRA calculation. The five heat structures considered in the simulation were vessel top head, cylindrical wall, internal components for aerosol, vessel bottom head, and internal components for aerosol settling. In the MELCOR calculation, aerosols can deposit on all surfaces; the surface areas are 63.0 m^2, 395.0 m^2, 232.0 m^2, 45.604 m^2, and 42.696 m^2, respectively. Therefore, the area summations of vessel bottom head and internal components for aerosol settling becomes the total sedimentation area of 88.3 m^2, and the area summations of vessel top head, cylindrical wall, and vessel bottom head becomes the total uncovered heat sink area of 503.6 m^2. Assuming that the temperatures of internal components are same as those of CSTF atmospheric temperature, the surface areas of internal components are not included in the total uncovered heat sink area on which thermophoretic deposition occurs. It was assumed that the outer walls of the heat structures were adiabatic except for the internal heat structure components for aerosol settling. In modeling test AB5, one non-radioactive aerosol component was used with 20 sections in the aerosol mass distribution. The minimum and maximum diameters for the aerosol size distribution, 0.01 and 10.0 μm, respectively, were taken from the test report. The aerosol source was modeled by specifying a log-normal distribution for the aerosol mass, using the reported values of 0.5 μm for the mass median diameter (MMD) and 1.5 for the geometric standard deviation (GSD). The input parameters used for the AB5 simulation by ISFRA and MELCOR codes are summarized in Table 4, in which the start time of the sodium spraying was set to be the time "0 s". Only the minimum and maximum time-steps for the MELCOR runs are given by users in Table 4, since the exact value of each time-step was controlled by the time-step control routine inside the MELCOR code. The sedimentation area and the uncovered heat sink area for the ISFRA runs were taken from the data in Table 1 of Souto et al. [18].

4.1.2. Results and discussion

Even though ABCOVE experimental research provided a range of measured aerosol data, such as suspended mass concentration (also called airborne mass), settled mass, plated mass, aerodynamic mass median diameter, geometric standard deviation of the particle size distribution, settling mean diameter, leaked mass, and instantaneous combined removal rate, only the suspended aerosol mass concentrations were used for the validation since the ISFRA aerosol analysis model using the FAI aerosol method can only calculate the total suspended aerosol mass and overall removal coefficient. The total suspended aerosol mass at 872 s, when the aerosol source rate became zero, was calculated from the measured aerosol concentration of 110 ± 17 g/m^3 to be 93.72 ± 14.48 kg, while the predicted values were 129.84 kg for the ISFRA run and 100.88 kg for the MELCOR run. Fig. 4(b) shows a comparison of the measured and the simulated suspended aerosol masses. The ISFRA and the MELCOR aerosol models estimate the suspended aerosol mass at 1020 s well within the standard error (1σ), while both models over-estimate the suspended aerosol masses at the later stage (11000~99900 s). Over-estimation of the suspended aerosol mass implies conservative evaluation, because the larger suspended aerosol mass would result in the larger source rates into the environment. Underestimation of suspended aerosol mass by the ISFRA aerosol model only appears in the transition period of 872~1100 s, when the atmospheric pressure and the shell and atmospheric temperature differences changed abruptly. The ISFRA simulation as well as the MELCOR simulation predicted the aerosol mass trend quite well: the suspended aerosol mass increased during the sodium spray fire

Table 4
Input data for simulating AB5 test.

Description	ISFRA	MAEROS (MELCOR)
CSTF TEST PARAMETER		
CSTF Total Height	20.3 m	
CSTF Cylinder Diameter	7.62 m	
CSTF Vessel Volume	852.0 m^3	
Sedimentation Area	88.3 m^2	88.3 m^2
Uncovered Heat Sink Area	503.6 m^2	503.6 m^2
CSTF Shell Temperature	Measured Value (See Fig. 4(a))	
GAS PARAMETER		
Ar Mole Fraction	0.01	0.0
Na Mole Fraction	0.0	0.0
N_2 Mole Fraction	0.8	0.767
H_2 Mole Fraction	0.0	0.0
O_2 Mole Fraction	0.19	0.233
Gas Viscosity	Air Property	
Gas Thermal Diffusivity	Air Property	
Gas Temperature	Measured Value (See Fig. 4(a))	
CSTF Atm. Pressure	Measured Value (See Fig. 4(a))	
AEROSOL PARAMETER		
Dynamic Shape Factor	1.5	
Agglomeration Shape Factor	2.25	
Slip Coefficient	1.37	
Sticking Coefficient	1.0	
Aerosol Particle Density	2500 kg/m^3	
Aerosol Diameter	_	0.01~10 μm
Number of Sections	_	20
Number of Aerosol Components	_	1
Aerosol Source Rate	0.445 kg/s (0~872 s) 0.0 kg/s otherwise	
Source aerosol MMD[a]	_	0.5 μm
Source Aerosol GSD[b]	_	1.5
CONTROL PARAMETER		
Initial Time	0.0 s	0.0 s
Maximum Time	513600.0 s	514000.0 s
Time Step	1~1000 s (user inputs)	0.01, 1 s (Δt_{min}, Δt_{max})

[a] Mass mean diameter.
[b] Geometric standard deviation.

period and then decreased steadily after the cessation of the sodium spraying. It should be noted that the starting time of sodium spraying was set to be the time "0 s" in Figs. 4 and 5.

Aerosol deposition by gravitational settling occurs on the sedimentation area, while thermophoretic deposition occurs on the uncovered heat sink area. The measured or calculated CSTF atmospheric and steel shell temperatures are major parameters affecting aerosol removal rates by thermophoretic deposition. Since these calculations using the stand-alone ISFRA aerosol program were not coupled with thermo-fluid calculations, some other important parameters for calculating the thermophoretic deposition were required as user input. As shown in Eqs. (28)–(30), the removal rate of thermophoretic deposition is proportional to the local Nusselt number. In the stand-alone ISFRA aerosol program the local Nusselt number (Nu_x) normalized by the characteristic length (L) are provided as input. Fig. 5 shows the comparison of the ISFRA predictions with different values of *Nu/L*. In the AB5 simulation using the original ISFRA computer code, where the CSTF atmosphere and shell temperatures are calculated by the code, *Nu/L* during the decaying period of 1000~100000 s ranged 10~130 m^{-1}. Since the sodium spray fire is not considered in the code calculation, the actual temperature difference between the CSTF atmosphere and steel shell is expected to be higher, as confirmed by measurements, and the corresponding *Nu/L* can be 150 m^{-1} or higher. Fig. 5 shows larger local Nusselt Numbers resulting in faster thermophoretic deposition velocities and higher aerosol removal rates. A *Nu/L* of 200, which gives the closest conservative prediction of the AB5 experiment, was selected as the base case.

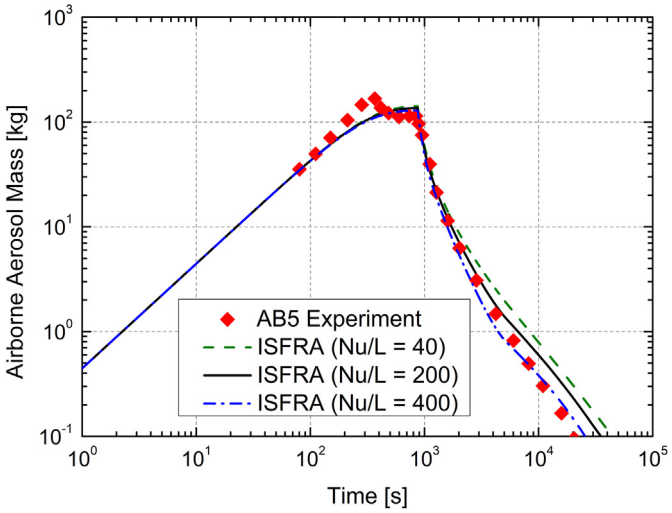

Fig. 5. Comparison of ISFRA calculations for the AB5 test with different *Nu/L* values.

This stand-alone aerosol module of ISFRA was utilized for the CPU time comparison between the MAEROS sectional method and the correlation-based log-normal aerosol model. Since this ISFRA aerosol module does not have the capability to analyze the multi-component aerosol behavior, CPU time comparison was performed only for the AB5 simulation. Table 5 compare the CPU times between the sectional and the correlation-based aerosol models in the ABCOVE AB5 prediction. For the CPU time comparison of basic logics only, the unnecessary procedures were removed and the simulation times were set to be the same value of 300000s. Both computations of the sectional and the correlation-based models were performed on the same PC with the 64-bit WINDOWS operating system on an Intel I7-7700 CPU. From this comparison result, it is concluded that the correlation-based aerosol model gives output about 80 times faster than the sectional method in the AB5 simulation.

4.2. *ABCOVE AB-6 test*

4.2.1. *Simulation models*

As discussed previously, test AB6 was performed in the same facility as test AB5 and, therefore, most of the geometric parameters required to model the CSTF vessel in test AB5 are applicable to test AB6. The external energy source in test AB6 was the sodium spray fire. This energy source includes both the energy released by chemical reactions, 2.86 GJ, and the sensible energy injected with the NaI source, 0.14 GJ [17]. The NaI aerosol source is reported to have a log-normal distribution with the MMD of 0.544 μm and the GSD of 1.55. The sodium combustion product aerosol, NaO_x, is also specified as a log-normal distribution with 0.5 μm and 2.0 for MMD and GSD, respectively.

For the ISFRA simulations of the AB6 test, an 852.0 m^3 control volume was modeled for the CSTF vessel. A single ISFRA run was performed for both NaI and NaO_x aerosols. The CSTF transient temperatures and pressures were also calculated as shown in Fig. 6(a). Fig. 6(a) also displays the calculated CSTF shell and atmosphere temperatures by the MELCOR runs, as well as the measured temperatures. The aerosol particle densities were specified as 3670 kg/m^3 and 2450 kg/m^3 for NaI and NaO_x aerosols, respectively. The NaI aerosol was generated at the rate of 0.00014 kg/s from 0 to 3000 s, and NaO_x aerosol was generated at the rate of 0.0779 kg/s from 620 to 5400 s.

Table 5
CPU time comparison between the sectional and the correlation-based aerosol models in the ABCOVE AB5 prediction.

	Stand-alone aerosol module of ISFRA code	MAEROS sectional model
Simulation condition	time_end = 300000.0 s	28 particle size sections time_end = 300000.0 s
CPU time	0.6250E-01 s	0.5000E+01 s

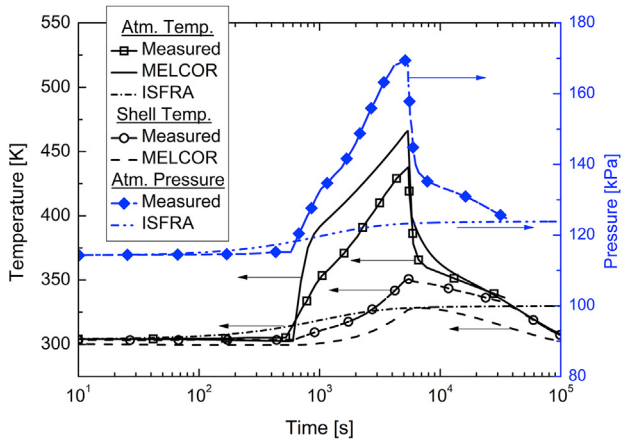

(a) CSTF atmosphere temperature, pressure, and shell temperature

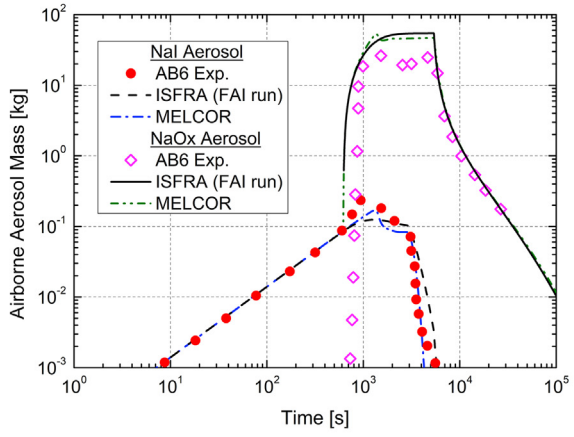

(b) Suspended aerosol mass inside the CSTF

Fig. 6. Validation condition and results for the AB6 test.

For the MELCOR simulations of the AB6 test, the CSTF vessel was modeled as a single control volume similar to the ISFRA run. Some thermal-hydraulic conditions, such as the heat structure and gas temperatures, and the vessel pressure, were provided as input, like the AB5 MELCOR simulation. This MELCOR simulation was a single calculation with two aerosol components: class 2 (alkali metals) for the NaO_x aerosol and new material class 16 for the NaI aerosol. Non-radioactive material was assumed in the case of NaO_x; on the other hand, NaI was assumed as radioactive material. The aerosol injection rates of NaO_x and NaI were same as in the ISFRA calculation. The minimum time step for MELCOR calculations over all time periods was set to 0.01 s. The maximum time-step was set to 1.0 s from 0 to 5400 s, the end of the sodium spray period, and 50 s from 5400 s to the end of the test. Table 6 presents the summary of the test AB6 parameters used in the ISFRA and MELCOR simulations.

4.2.2. Results and discussion

Test AB6 simulated an accident in which the FP NaI is released in the presence of a sodium spray fire, which releases sodium combustion product aerosols. The chemical form of this aerosol was a mixture of sodium peroxide (Na_2O_2) and sodium hydroxide (NaOH). To simplify discussions, the aerosol formed by the sodium spray fire is referred to as NaO_x in this work.

Fig. 6(b) shows the measured suspended aerosol masses of NaO_x and NaI and the corresponding simulation results of MELCOR and ISFRA. The measured NaO_x airborne mass rapidly increases to a maximum value of 28.l kg at about 1220 s. It then slowly decreases to 19.6 kg. Near the end of the NaI release period (3000 s), it increases again to a 23.9 kg. After the NaO_x source was turned off at 5400 s, the suspended mass decreased rapidly.

Both the ISFRA and MELCOR results followed similar trends, but they over-predicted the NaO_x airborne mass by a factor of 1.3~1.6 during the NaO_x source release period of 620~5400 s. At 1225 s, the ISFRA and MELCOR predicted the maximum NaO_x airborne mass of 37.2 kg and 45.5 kg, respectively, while the measured maximum aerosol mass was about 28.1 kg. About 10 min after the end of the sodium spray, the ISFRA and MELCOR predictions were in good agreement with the experimental results.

The NaI source started at time zero and ended at 3000 s. The measured NaI airborne mass increased to a maximum of 0.23 kg, attained at about 900 s, and then decreased to 0.07 kg at the end of the NaI source period. Immediately after the NaI source was turned off, the airborne mass decreased rapidly. In Fig. 6(b), both the ISFRA and the MELCOR results showed reasonably good agreement with experimental results during the NaI source release period. The calculated maximum of the ISFRA simulation was 0.12 kg at 1300 s, and then the predicted NaI mass decreased gradually. The calculated maximum of the MELCOR simulation was 0.17 kg at 1323 s, and then the predicted NaI mass decreased to 0.083 kg approximately 200 s before the end of the source period. In comparison with the measured maximum NaI aerosol mass of 0.23 kg, MELCOR under-predicted the maximum suspended NaI aerosol mass by approximately 26%. On the other hand, ISFRA under-predicted the maximum suspended NaI aerosol mass by approximately 46%.

The measured NaI suspended mass is presented with the corresponding ISFRA and MELCOR results in Fig. 6(b). The so-called “washout” effect [16,17] of the FP aerosol NaI by the continuing source of the NaO_x aerosol is observed from the transient NaI aerosol masses after 620 s when the NaO_x aerosol generation starts. After 620 s, until the NaI source termination, the NaO_x source continued at constant rate. The NaI particles agglomerated with the much more abundant NaO_x particles, causing a rapid shift of the NaI size distribution to larger sizes. The larger particles settle on the surfaces faster than the smaller ones. The measured mass ratio decayed very rapidly, because the agglomeration of the NaI particles with the NaO_x particles increased the settling of NaI aerosols by gravity.

Both the ISFRA and MELCOR results followed this rapid decay of NaI aerosol between 620 and 3000 s. In the ISFRA and MELCOR calculations the aerosol agglomeration process was simulated between two species, NaI and NaO_x. In the simulation results, “washout” of the NaI aerosol started with the commencement of

Table 6
Input data for simulating AB6 test.

Description	ISFRA	MAEROS (MELCOR)
CSTF TEST PARAMETER		
CSTF Total Height	20.3 m	
CSTF Cylinder Diameter	7.62 m	
CSTF Vessel Volume	852 m^3	
Sedimentation Area	88.3 m^2	88.3 m^2
Uncovered Heat Sink Area	503.6 m^2	503.6 m^2
CSTF Shell Temperature	Measured Value (See Fig. 6(a))	
GAS PARAMETER		
Ar Mole Fraction	0.0	0.0
Na Mole Fraction	0.0	0.0
N_2 Mole Fraction	0.8	0.761
H_2 Mole Fraction	0.0	0.0
O_2 Mole Fraction	0.2	0.239
Gas Viscosity	Air Property	
Gas Thermal Diffusivity	Air Property	
Gas Temperature	Measured Value (See Fig. 6(a))	
CSTF Atm. Pressure	Measured Value (See Fig. 6(a))	
AEROSOL CONSTANT		
Dynamic Shape Factor	1.0	
Agglomeration Shape Factor	2.5	
Slip Coefficient	1.37	
Sticking Coefficient	0.33	
NaI Aerosol Particle Density	3670 kg/m^3	3670 kg/m^3
NaI Aerosol Source Rate	0.00014 kg/s (0~3000 s) 0.0 kg/s otherwise	
NaI Aerosol Source MMD	_	0.544 μm
NaI Aerosol Source GSD	_	1.55
NaO_x Aerosol Particle Density	2450 kg/m^3	3670 kg/m^3
NaO_x Aerosol Source Rate	0.0779 kg/s (620~5400 s) 0.0 kg/s otherwise	
NaO_x Aerosol Source MMD	_	0.5 μm
NaO_x Aerosol Source GSD	_	2.0
CONTROL PARAMETER		
Simulation Type	Single Run with 2 Aerosol Components	
Initial Time	0.0 s	0.0 s
Maximum Time	513600.0 s	277000.0 s
Time Step	1~1000 s (user inputs)	0.01, 50 s (Δt_{min}, Δt_{max})

NaO_x injection at 620 s, when the aerosol removal rate of NaI increased due to the agglomeration with NaO_x aerosols having a higher generation rate than the NaI aerosol. In the case of NaO_x decay, similar results were shown in both the ISFRA and MELCOR results after about 6000 s, as reflected in Fig. 6(b). In this late period, there is a small amount of NaI in the vessel, and interaction between two aerosol species did not occur.

The small difference between the ISFRA and MELCOR results can be explained by the difference in the aerosol particle density. In the MELCOR calculation, the sectional method was used to calculate aerosol behavior such as agglomeration and deposition. In the MELCOR input, only a single density value can be employed without distinguishing the aerosol species. In the AB6 experiment simulation, the aerosol density of 3670.0 kg/m^3 was solely considered to calculate the aerosol behavior even though two different aerosols were used.

4.3. ABCOVE AB-7 test

4.3.1. Simulation models

Test AB7 is similar to test AB6 but with smaller sources. The energy sources in test AB7 are the small sodium pool fire, which is the energy released by the chemical reaction to produce sodium hydroxide, NaOH, as well as the sensible energy from the Na source. The energy from the chemical reaction is 4.98×10^7 J, whereas the sensible energy is 4.73×10^6 J [18]. The NaOH aerosol source is reported to have a log-normal particle size distribution with mass median diameter of 0.5 μm and GSD of 2.0. The NaI aerosol source is reported to have a log-normal particle size distribution with the mass median diameter of 0.54 μm and GSD of 1.55.

For the ISFRA simulations of the AB7 test, a single ISFRA run was performed for both NaOH and NaI aerosols. The time-dependent CSTF transient temperatures and pressures shown in Fig. 7(a) were provided as inputs. Fig. 7(a) also shows the calculated CSTF shell and atmosphere temperatures by the MELCOR runs, assuming that all the injected sodium had been converted into NaOH during the leak period of 600 s. The aerosol particle densities were specified as 2130 kg/m^3 and 3670 kg/m^3 for the NaOH and NaI aerosols, respectively. The NaOH aerosols were introduced at the rate of 0.00503 kg/s from 0 to 600 s. The NaI aerosols were introduced at the rate of 0.000197 kg/s from 600 to 2400 s.

In Figs. 4(a) and 6(a) and 7(a), the MELCOR predictions overestimated the atmospheric temperatures during the sodium spray/pool fire periods. Since 2013, SFR-capabilities of the MELCOR code had been developed by implementing the sodium properties data from the SIMMER-III, and the containment sodium fire models and the sodium atmospheric chemistry from the CONTAIN-LMR code [21]. However, it was proven in a previous study that the discrepancies between the atmosphere temperature computed by MELCOR and the experimental values for AB5, AB6, and AB7 were caused by not using proper sodium spray/pool fire models in the MELCOR predictions [22].

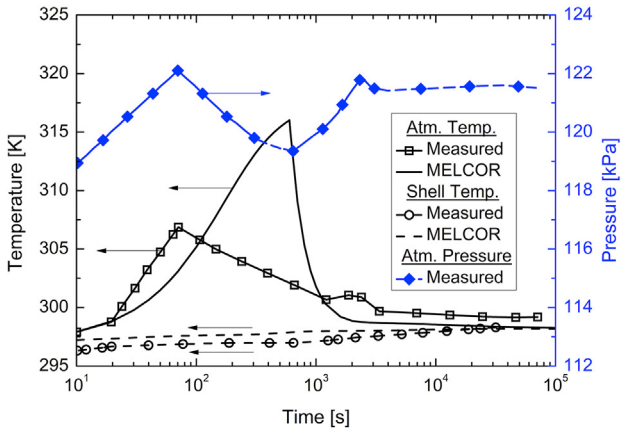

(a) CSTF atmosphere temperature, pressure, and shell temperature

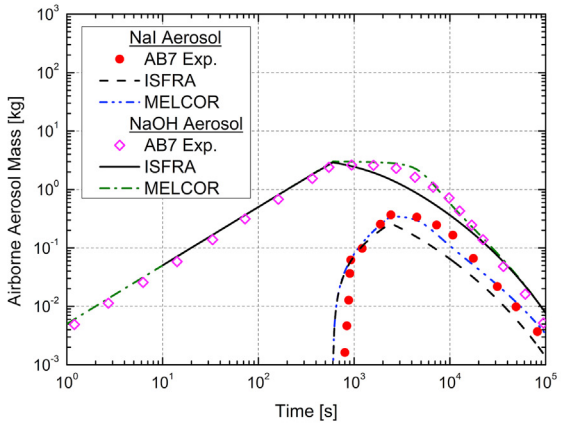

(b) Suspended aerosol mass inside the CSTF

Fig. 7. Validation condition and results for the AB7 test.

For the MELCOR simulations of the AB7 test, the CSTF vessel was modeled as a single control volume. Similar to the AB5 and AB6 conditions, the measured heat structure temperature data were provided in the input. This MELCOR simulation was a single calculation with two aerosol components of MELCOR default class 2 (alkali metals) for the NaOH aerosol and new material class 16 for the NaI aerosol. The minimum time-step over all time periods was set to 0.01 s. The maximum time-step was 10 s during the entire period of calculation. Table 7 presents the summary of test AB7 parameters used in the ISFRA and the MELCOR calculations.

4.3.2. Results and discussion

The purpose of test AB7 was to provide experimental data to validate aerosol behavior codes in the case of agglomeration of two groups of aerosols, simulating the release of a FP, NaI, after the end of a small sodium pool fire [18].

All of the sodium oxide released during the sodium pool fire reacted with the moisture in the CSTF vessel atmosphere to produce sodium hydroxide (NaOH) aerosols. The duration of the pool fire, and therefore the NaOH source period, was approximately 600 s. The NaI aerosol source began at the end of the NaOH source, 600 s, and ended at 2400 s.

The measured NaOH airborne mass and the corresponding ISFRA and MELCOR calculations are presented in Fig. 7(b). The measured NaOH airborne mass increased to a maximum of 2.56 kg at the end of the NaOH source period, remained constant for the next 1400 s, and then decreased slowly. The MELCOR calculations followed a very similar trend throughout the entire test period, while the ISFRA calculations followed a very similar trend up to 600 s, after which the calculated airborne NaOH mass decreased gradually without any plateau period. The maximum NaOH airborne mass estimated by the ISFRA calculation is 2.91 kg at 600 s, representing an over-prediction of about 13.7%, while that of the MELCOR calculation is 3.0 kg at 600 s, representing an over-prediction of about 17%.

Table 7
Input data for simulating AB7 test.

Description	ISFRA	MAEROS (MELCOR)
CSTF TEST PARAMETER		
CSTF Total Height	20.3 m	
CSTF Cylinder Diameter	7.62 m	
CSTF Vessel Volume	852 m^3	
Sedimentation Area	88.3 m^2	88.3 m^2
Uncovered Heat Sink Area	503.6 m^2	503.6 m^2
CSTF Shell Temperature	Measured Value (See Fig. 7(a))	
GAS PARAMETER		
Ar Mole Fraction	0.01	0.0
Na Mole Fraction	0.0	0.0
N_2 Mole Fraction	0.8	0.7905
H_2 Mole Fraction	0.0	0.0
O_2 Mole Fraction	0.19	0.2095
Gas Viscosity	Air Property	
Gas Thermal Diffusivity	Air Property	
Gas Temperature	Measured Value (See Fig. 7(a))	
CSTF Atm. Pressure	Measured Value (See Fig. 7(a))	
AEROSOL CONSTANT		
Dynamic Shape Factor	1.5	
Agglomeration Shape Factor	2.25	
Slip Coefficient	1.37	
Sticking Coefficient	1.0	
NaI Aerosol Particle Density	3670 kg/m^3	3670 kg/m^3
NaI Aerosol Source Rate	0.000197 kg/s (600~2400 s) 0.0 kg/s otherwise	
NaI Aerosol Source MMD	_	0.54 μm
NaI Aerosol Source GSD	_	1.55
NaOH Aerosol Particle Density	2130 kg/m^3	3670 kg/m^3
NaOH Aerosol Source Rate	0.00503 kg/s (0~600 s) 0.0 kg/s otherwise	
NaOH Aerosol Source MMD	_	0.5 μm
NaOH Aerosol Source GSD	_	2.0
CONTROL PARAMETER		
Simulation Type	Single Run with 2 Aerosol Components	
Initial Time	0.0 s	0.0 s
Maximum Time	513600.0 s	162000.0 s
Time Step	1~1000 s (user inputs)	0.01, 10 s (Δt_{min}, Δt_{max})

The measured NaI airborne mass as a function of time, together with the ISFRA and MELCOR calculated results, are presented in Fig. 7(b). The measured NaI airborne mass increased to a maximum of 3.58×10^{-1} kg at the end of the NaI source period (2400 s), remained constant for 1400 s, and then decreased slowly. The MELCOR results closely followed the experimental measurements throughout the full period of the test. On the other hand, ISFRA predicted the measured airborne aerosol mass reasonably well during the source period but slightly over-predicted the decay after the source was turned off. In the modeling two aerosol species in a single run, the ISFRA run might over-estimated the agglomeration effect. The maximum NaI airborne mass estimated by the ISFRA calculations was 2.63×10^{-1}kg at 2400 s, representing an under-prediction by 28.5%, while that by MELCOR calculations was 3.48×10^{-1} kg at 2400 s, representing an under-prediction by 2.8%.

Although there is an interaction between different aerosol groups in the AB7 test, separate ISFRA calculations for each aerosol group gave reasonable, somewhat conservative prediction of the measured data. MELCOR results were in good agreement with the measurements.

5. Conclusions

The purposes of this study were to investigate the validity of the aerosol model in the ISFRA computer program and to benchmark the ISFRA aerosol model against the ABCOVE experiments. In Section 2, theoretical basis of the correlation technique used in the ISFRA aerosol model was reviewed. Compare to the sectional method, it was demonstrated that the ISFRA aerosol model could provide a fast and stable calculations for most of the cases unless the aerosol size distribution is strongly affected by processes other than agglomeration and gravitational settlement such as: hygroscopic aerosols, aerosols emerging from suppression pool, and evaporation of aerosols in dry atmosphere. Currently only the total suspended and deposited aerosol masses without any information of aerosol particle size distributions are available in the ISFRA output. The particle size distribution used for the calculation is also available inside the code and can easily be made output in the next version of the code.

In Sections 3 and 4 the ISFRA aerosol model was validated against the ABCOVE AB5, AB6, and AB7 tests, as well as against the MELCOR results. The validation proved that the ISFRA aerosol models can predict the suspended aerosol masses of the single-species aerosol test (AB5) and the multi-species aerosol test with weak interaction between the different aerosol groups (AB7) with reasonable agreement with the experimental data, at about the same level of accuracy as MELCOR. Moreover, it was also revealed that the ISFRA aerosol models could predict the suspended aerosol masses of the multi-species aerosol test with strong interaction between the two different aerosol species (AB6) as accurately as the MELCOR code.

In this study, the characteristics and limitations of the ISFRA aerosol model were identified.

Declaration of competing interest

The authors declare that they have no known competing financial interests or personal relationships that could have appeared to influence the work reported in this paper.

Acknowledgment

This research has been supported by the National Research Foundation of Korea (NRF) grant funded by the Korea government (MSIT). (No. 2021M2E2A1037871).

Nomenclature

c_1, c_2, c_3	coefficients used in dimensional analysis
C_m	Cunningham slip correction factor
d_1, d_2, d_3	coefficients used in dimensional analysis
d_p	aerosol particle diameter [m]
E	efficiency of inertial deposition
f	friction factor for turbulent flow
g	gravitational constant
h	effective height for aerosol deposition [m]
j	particle deposition flux [particles/m^2/s]
k	Boltzmann constant
K	kernel representing the frequency of binary collisions between particles
K_0	normalized Brownian collision coefficient ($= 4kT/(3\mu)$)
m	total mass concentration of the suspended aerosols [kg/m^3]
m_{SS}	expected steady-state airborne aerosol mass concentration [kg/m^3]
$\dot{m}_p$	aerosol mass production rate [kg/m^3/s]
M	dimensionless total suspended aerosol mass
$\dot{M}_p$	dimensionless source rate
n	particle size distribution function [m^{-3}]
$\dot{n}_p$	source rate of particles [m^{-3}s^{-1}]
N	dimensionless particle distribution function
Nu_x	local Nusselt number $\left(= \frac{x(\partial T/\partial y)_{y=0}}{(T_\infty - T_w)} \right)$
Pr	Prandtl number
Sh_x	local Sherwood number for particle deposition (Eq. (27))
t	time [s]
T	carrier gas temperature [K]
u	particle deposition or removal velocity [m/s]
u_g	carrier gas velocity [m/s]
v	particle volume [m^3]
x	coordinate along the vertical plate [m]
y	coordinate normal to the plate [m]

Greek letters

α	density correction factor
β	dimensionless thermophoretic velocity coefficient
χ	particle settling shape factor
ε	capture coefficient
γ	collision shape factor
λ	aerosol removal rate constant [s^{-1}]
Λ	dimensionless decay constant
μ	viscosity of the carrier gas [kg/m/s]
μ_g	carrier gas viscosity [kg/m/s]
ρ	density of the aerosol material [kg/m^3]
ρ_g	carrier gas density [kg/m^3]
σ	standard deviation (error)
τ	dimensionless time
ν	dimensionless particle volume

Superscripts

D	decaying aerosol
SS	steady-state

Subscripts

B	Brownian (coagulation)
DIF	diffusiophoresis
g	gravitational (coagulation)
IMP	inertial impaction
L	leakage
SED	sedimentation
TH	thermophoresis
TOT	total
w	at the wall (plate surface)
∞	outside the free convection boundary layer.

References

[1] J. Yoo, J. Chang, J.-Y. Lim, J.-S. Cheon, T.-H. Lee, S.K. Kim, K.L. Lee, H.-K. Joo, Overall system description and safety characteristics of Prototype gen IV sodium cooled fast reactor in Korea, Nuclear Engineering and Technology 48 (2016) 1059–1070.
[2] Fauske, L.L.C. Associates, ISFRA User Manual, FAI Report, FAI/16-1089, 2016, p. 10.
[3] M. Epstein, P.G. Ellison, R.E. Henry, Correlation of aerosol sedimentation, J. Colloid Interface Sci. 113 (No. 2) (1986).
[4] M. Epstein, P.G. Ellison, A principle of similarity for describing aerosol particle size distribution, J. Colloid Interface Sci. 119 (No. 1) (1987) 168–173.
[5] M. Epstein, P.G. Ellison, Correlations of the rate of removal of coagulating and depositing aerosols for application to nuclear reactor safety problems, Nucl. Eng. Des. 107 (1988) 327–344.
[6] M. Epstein, G.M. Hauser, R.E. Henry, Thermophoretic deposition of particles in natural convection flow from a vertical plate, J. Heat Tran. 107 (1985) 272–276.
[7] R.K. Hilliard, J.D. McCormack, A.K. Postma, Results and code predictions for ABCOVE aerosol code validation - test AB5, HEDL-TME 83–16 (1983).
[8] R.K. Hilliard, J.D. McCormack, L.D. Muhlstein, Results and code predictions for ABCOVE aerosols code validation - test AB-6 with two aerosol species, HEDL-TME 84–19 (1984).
[9] R.K. Hilliard, J.D. McCormack, L.D. Muhlestein, "Results and code predictionsfor ABCOVE aerosol code validation with low concentration NaOH and NaI aerosol – CSTF test AB7, HEDL-TME 85–1 (1985).
[10] N.A. Fuchs, The Mechanics of Aerosols, Pergamon, Oxford, 1964.
[11] F.M. White, Fluid Mechanics, third ed., McGraw-Hill, Inc., NJ, USA, 1994. Chap. 5.
[12] F. Gelbard, Y. Tambour, J.H. Seinfeld, Sectional representations for simulating aerosol dynamics, J. Colloid Interface Sci. 76 (1980) 541–556.
[13] F. Gelbard, The MAEROS User Manual, NUREG/CR-1391, SAND80-0822, Sandia National Labs Report, 1982.
[14] OECD/NEA Data Bank, http://oecd-nea.com/.
[15] FAI, "Technical Support for Issue Resolution," FAI/85-27, Fauske & Associates, Inc., 1985.
[16] E.H. Ryu, "Confirmation of Epstein's Correlations for the Rate of Removal of Coagulating and Depositing Aerosols", KAERI Technical Report, KAERI/TR-6859/2017, 2017 (In Korean).
[17] W.H. Press, B.P. Flannery, S.A. Teukolsky, W.T. Vetterling, Numerical Recipes in FORTRAN: the Art of Scientific Computing, Cambridge University Press, 1992.
[18] F.J. Souto, F.E. Haskin, L.N. Kmetyk, MELCOR 1.8.2 Assessment: Aerosol Experiments ABCOVE AB5, AB6, AB7, and LACE LA2," SAND94-2166, 1994.
[19] L.E. Herranz, M. Garcia, S. Morandi, Benchmarking LWR codes capability to model radionuclide deposition within SFR containments: an analysis of the Na ABCOVE tests, Nucl. Eng. Des. 265 (2013) 772–784.
[20] K.S. Ha, S.I. Kim, J.-S. Jang, D.H. Kim, "Code Development on Fission Product Behavior under Severe Accident – Validation of Aerosol Sedimentation, " KNS Spring Meeting, Jeju, Korea, 2016.
[21] L. Humphries, B. Beeny, D. Louie, H. Esmaili, M. Salay, Non-LWR Model Development for the MELCOR Code," ICONE26-82415, July 2018. London, England.
[22] C. Yoon, S.J. Ahn, S.H. Kang, Validation of the Sodium Fire Models in the CONTAIN-LMR/1B-Mod.1 Code against the ABCOVE Experiments, " KNS Spring Meeting, Jeju, Korea, May 2019.